JACS
JOURNAL OF THE AMERICAN CHEMICAL SOCIETY
pubs.acs.org/JACS
Article

Early Folding Dynamics of i-Motif DNA Revealed by pH-Jump Time-Resolved X-ray Solution Scattering

Arnold M. Chan, Sasha B. Ebrahimi, Devleena Samanta, Denis Leshchev, Adam K. Nijhawan, Darren J. Hsu, Madeline B. Ho, Namrata Ramani, Irina Kosheleva, Robert Henning, Chad A. Mirkin, Kevin L. Kohlstedt,* and Lin X. Chen*

Cite This: J. Am. Chem. Soc. 2024, 146, 33743−33752

ABSTRACT: The i-motif is a pH-responsive cytosine-rich oligonucleotide sequence that forms, under acidic conditions, a quadruplex structure. This tunable structural switching has made the i-motif a useful platform for designing pH-responsive nanomaterials. Despite the widespread application of i-motif DNA constructs as biomolecular switches, the mechanism of i-motif folding on the atomic scale has yet to be established. We investigate the early folding structural dynamics of i-motif oligonucleotides with laser-pulse-induced pH-jump time-resolved X-ray solution scattering. Following the pH-jump, we observe that the initial random coil ensemble converts into a contracted intermediate state within 113 ns followed by further folding on the 10 ms time scale. We reveal the representative structures of these transient species, hitherto unknown, with molecular dynamics simulations and ensemble fitting. These results pave the way for understanding metastable conformations of i-motif folding and for benchmarking emerging theoretical models for simulating noncanonical nucleic acid structures.

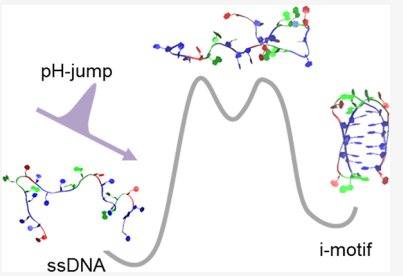

INTRODUCTION

Responsible for carrying genetic information, canonical B-DNA has a well-known double helical structure; however, nucleic acids can adopt a myriad of other structural conformations, giving them a wide variety of functions depending on their environment. Studying the diverse structures of nucleic acids is important to understanding mechanisms in biological activity and programmable nanotechnology.[1−4] Among the many dynamic DNA systems, i-motifs have been used to drive DNA structural assembly and function due to their pH-responsive conformational switching.[5] The i-motif is a cytosine-rich sequence that forms an antiparallel intercalated quadruplex structure via hemiprotonated C:C+ base pairs[6] (Figure 1, bottom). Their ability to act as tunable switches between extended single-stranded structures and collapsed quadruplexes has made i-motifs widely used moieties in pH sensors and dynamic nanodevices.[1,7−10] Furthermore, human telomere regions that contain sequences for gene transcription and maintenance are comprised of cytosine-rich tandem repeats, capable of forming i-motifs.[11] There is increasing evidence of cytosine-rich regions in human cells that form i-motif quadruplexes at neutral pH *in vitro*, although their direct epigenetic role *in vivo* is still debated.[12,13] The physiological relevance of i-motif DNA and its utility as a programmable biomacromolecule necessitate a deeper molecular understanding of its relevant functional and structural dynamics.

Non-Watson−Crick−Franklin (Hoogsteen) base-pairing structural dynamics and folding mechanisms are of emerging interest in both experimental and computational biophysical studies.[14−17] Researchers have previously looked at i-motif formation and stabilization by considering various factors such as cytosine content, capping interactions, and ion interactions.[16,18−20] Several studies have analyzed the stability of the quadruplex structure and its transition under steady-state conditions.[15,16,21] i-Motif sequences with longer consecutive cytosine groups had higher melting temperatures than those with shorter ones (similar to duplexed DNA where longer duplexes generally have higher melting temperatures than shorter ones).[22,23] Yet, the kinetics of the structural transitions of i-motif over a range of pH values has largely been unexplored, which has hindered the understanding of the dynamics during rational design of i-motif into programmable nanomachines.[24] Initial work that broadly characterized i-motif structural transitions utilized conventional UV−visible absorbance and circular dichroism spectroscopy to track the i-motif Hoogsteen base pair content spanning a pH range.[20,25] In order to extract more direct information about the biochemical structure, experiments with better local spatial sensitivity were implemented.[14,26] Using single-molecule FRET, researchers have shown that metastable intermediate i-motif structures

Received: August 26, 2024
Revised: November 18, 2024
Accepted: November 19, 2024
Published: November 28, 2024

https://doi.org/10.1021/jacs.4c11768
J. Am. Chem. Soc. 2024, 146, 33743−33752

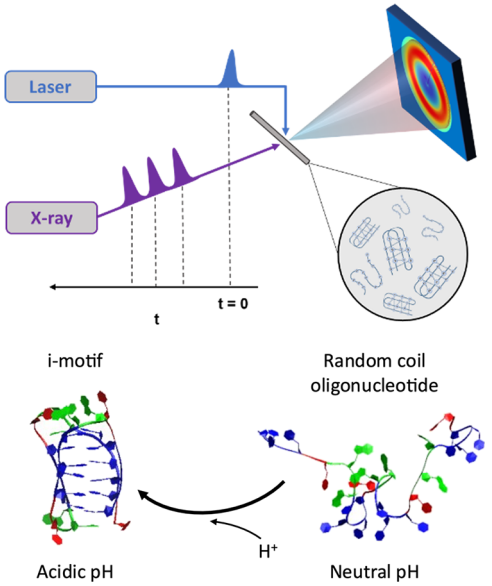

Figure 1. (top) Schematic illustration of the pH-jump pump-probe TRXSS experimental setup: UV laser pulses perpendicularly overlapped with time-delayed X-ray pulses on the sample capillary flow-cell. (bottom) In response to acidic conditions, i-motif folding is triggered upon protonation of cytosines (colored in blue).

exist, especially closer to the conformational transition pH threshold.[14,27] Using NMR spectroscopy, Gonzalez and co-workers showed the role of terminal minor groove tetrads (G:C:G:C) in forming different i-motif structures via interactions with the noncytosine nucleotides in the sequence.[16] These discoveries highlight efforts toward understanding the environmental and intrinsic conditions of i-motif conformational switching under equilibrium conditions. However, dynamic structural characterizations directly revealing the mechanism or pathway of i-motif folding have remained elusive. Emerging computational methodologies with all-atom molecular dynamics (MD) simulations have been employed to characterize the key conformational barriers, but determining the folding pathway of i-motifs remains a challenge to resolve without intentionally steering the corresponding cytosines to connect.[17,28,29]

In this work, we investigate the pH-dependent folding mechanism of i-motifs by probing the conformational dynamics on the nanosecond to millisecond time scales using time-resolved X-ray solution scattering (TRXSS) (Figure 1, top). In the past decade, instrumentation has been developed at advanced X-ray light sources, such as third-generation synchrotrons, to carry out time-resolved structural studies using the "pump-probe" approaches replacing the optical probe pulses with X-ray pulses, to directly characterize protein and nucleic acid structure through either elastic or inelastic X-ray scattering and X-ray spectroscopies.[30−38] The pH-dependent TRXSS we have developed utilizes this instrumentation to trigger the pH-dependent folding of the i-motif. We use an i-motif sequence that contains 21 nucleotides and allows for the exploration of various flexible conformations facilitated by the core i-motif with three-nucleotide long cytosine tracts. To capture its global structural information without relying on biochemical modifications to the oligonucleotide, small-/wide- angle X-ray solution scattering (S/WAXS) is a suitable probe established for resolving the shapes and sizes of biomolecules.[39−41] To capture dynamic structural changes due to environmental changes, e.g., pH-jump, it is necessary to use TRXSS to collect structural information during the pH-induced folding process. By coupling X-ray solution scattering with a laser-induced trigger, various time-resolved experiments have been constructed to measure protein structural dynamics resulting from temperature-jump, pH-jump, or light-induced chemical reactions.[32−34,42,43] Recent advances in the structural interpretation of biomolecular SAXS signals have permitted the modeling of the measured signals with atomistic models, further enumerating the biophysical information extracted beyond local spectroscopic probes.[35,44] We report the first pH-jump TRXSS experiment on a nucleic acid system that looks at nanosecond to millisecond structural dynamics. Complementary MD simulations and analysis methods were used to provide atomically detailed structural models for the species-associated signals extracted from the TRXSS data, accounting for the conformational flexibility of the i-motif DNA. Thus, our combined experimental and computational approach for characterizing the early steps of pH-induced i-motif formation revealed previously unknown transient conformations as well as their relevant chronology in the folding mechanism.

EXPERIMENTAL SECTION

Oligonucleotide Synthesis. The i-motif DNA oligonucleotide 5′-CCC TAA CCC TAA CCC TAA CCC TAA CCC-3′ was synthesized and purified using standard desalting procedures. The oligonucleotide sample was lyophilized and stored at −20 °C until needed for the respective experiments. Full synthetic details are available in the Supporting Information.

Equilibrium pH-Dependent SAXS. The i-motif DNA was dissolved in 10 mM phosphate buffer with 140 mM sodium chloride to a concentration of 2.5 mg/mL. The pH was adjusted with small amounts of 1 M sodium hydroxide or hydrochloric acid until all pH values were reached in the reported series. The samples were then heated to 95 °C for 5 min and cooled to room temperature. The solutions were filtered through a 0.2-μm syringe filter immediately before the SAXS measurements. The equilibrium SAXS data was collected at the DuPont-Northwestern-Dow Collaborative Access Team (DND-CAT) beamline at Sector 5 of the Advanced Photon Source (APS) at Argonne National Laboratory. During data acquisition, the sample was flowed continuously through a 1.5 mm glass capillary at a flow rate of 20 μL/s. Solution scattering data were collected for the i-motif DNA solution and corresponding buffer at an X-ray energy of 10 keV for 10 frames of 2-s exposure each. Data reduction and processing details are reported in the Supporting Information.

pH-Jump TRXSS. The TRXSS experiments were performed at the BioCARS beamline at the APS. Details of the pump-probe TRXSS instrumentation and general data acquisition modes have been previously reported.[45,46] This study follows the same methodology as previous pH-jump TRXSS experiments: a horizontally mounted glass capillary, coupled with a syringe pump, was the sample delivery system.[31,43,44,47] The i-motif sequence oligonucleotide was dissolved in deionized water with 150 mM sodium chloride and 8 mM o-nitrobenzaldehyde to a concentration of 2.5 mg/mL. Small amounts of 0.1 M sodium hydroxide or hydrochloric acid were added to the solution until a pH of 6.8 was reached. The solution was warmed to 95 °C for five min and allowed to cool to room temperature before filtering with a 0.2-μm syringe filter. The pH-jump was triggered by delivering 7 ns laser pulses at 315 nm to photoexcite the o-nitrobenzaldehyde photoacid. The UV laser pulse was focused to a beam size of 125 μm × 440 μm with a pulse power density of 22.7 mJ/mm^2 at the focal spot, approximately 6.5 μJ per pulse. The overlapping X-ray probe beam was focused to 30 × 35 μm. TRXSS profiles were collected at various time delays ranging from 300 ns to 50 ms with different probe pulse durations (100 ps, 500 ns, or 3.7 μs

https://doi.org/10.1021/jacs.4c11768
J. Am. Chem. Soc. 2024, 146, 33743−33752

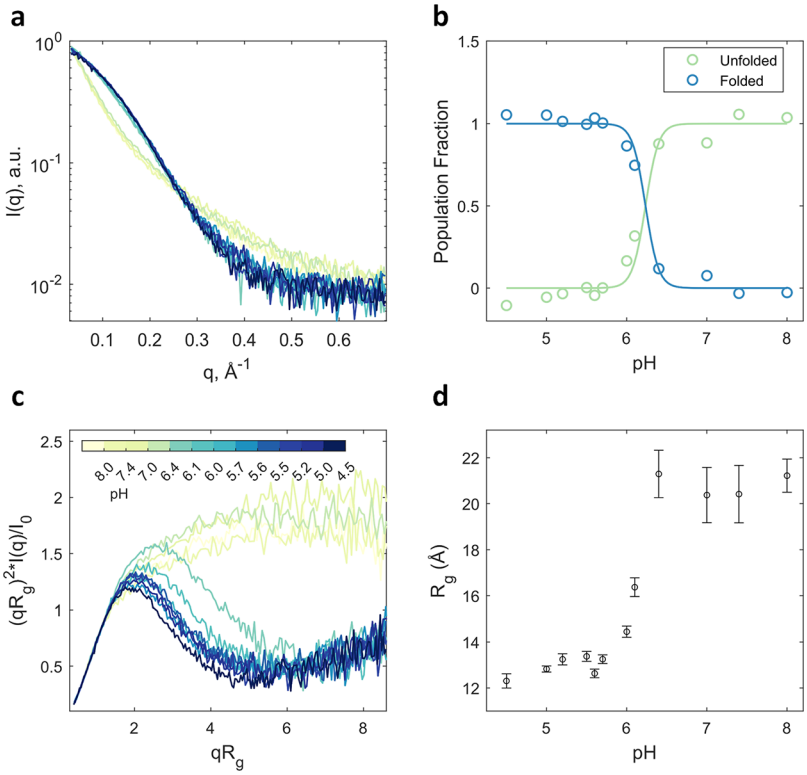

Figure 2. pH-Dependent equilibrium SAXS results. (a) Equilibrium SAXS profiles for i-motif oligonucleotide pH series. (b) Population fractions of the two-state folded/unfolded species from pH 4.5 to 8.0. (c) Dimensionless Kratky plot of the i-motif DNA pH series. (d) Experimental ensemble R_g with standard errors for each corresponding pH.

with different opening times of the X-ray shutter) to optimize data acquisition. The scattered X-rays were collected with a Rayonix MS340-HS detector placed 362 mm from the capillary. Details regarding the data processing are reported in the Supporting Information.

Molecular Dynamics Simulations. To sufficiently sample the conformational landscape of the i-motif oligonucleotide, three molecular dynamics trajectories (40 ns at high temperature and 20 ns at low temperature) were generated to create atomistic structural models. For all the simulations, the AmberTools18 package and the tleap program were used to create the initial coordinate and topology files.[48] The Amber force field for nucleic acids ff99 with the bsc1 adaptations for protonated cytosines was chosen, according to the methodology established by Wolski and co-workers.[17,29,49] Each initial structure was solvated in a periodic cubic TIP3P water box padded by 10 Å in all dimensions, and Na+ or Cl− counterions were added to appropriately neutralize the charge. The simulations started from the initial hemiprotonated i-motif structure (PDB ID: 1EL2), published by Phan and Mergny,[50] and the OpenMM engine was used.[51] One of the high-temperature (800 K) simulations started from the deprotonated i-motif with canonical cytosines, while the other two (one at 298 K low temperature and another at high temperature) used the hemipotonated i-motif. The integration time step for all the simulations was 2 fs, and Langevin dynamics was employed with a damping coefficient of 1 ps^{-1}. The system was minimized to generate a well-behaved starting structure and then was run in the NPT ensemble with a Monte Carlo barostat to maintain a hydration layer similar to those under TRXSS conditions. For all three simulations, the energies were minimized and the simulations were run for at least 20 ns.

Ensemble Optimization Structural Modeling. Theoretical X-ray solution scattering patterns were calculated for each candidate structure from the MD simulations using a protocol published by our group based on the FoXS methodology.[52] Each of the 800 K trajectories (fast dynamics) was sampled in 20 fs increments, while the 298 K trajectory (slow dynamics) was sampled every 40 fs, resulting in oligonucleotide structure pools of 1000 and 500 frames, respectively. Details on the conformational diversity of these trajectories are reported in the Supporting Information (Figure S12). One thousand independent conformations from the deprotonated oligonucleotide trajectory were used as candidate structures for modeling the unfolded species (U) prior to the experimental pH-jump. One thousand individual conformations from the high-temperature protonated oligonucleotide trajectory and an additional 500 conformations from the low-temperature trajectory were used as candidate structures for modeling both the transient intermediate (I) and transient folded species (F). For each of the kinetic species, a genetic algorithm was used to optimally obtain groups of conformations whose calculated theoretical average would most closely match its species-associated experimental X-ray scattering signal.[44,53,54] Each group of conformations is referred to as a "chromosome," consisting of 30 theoretically calculated and appropriately scaled X-ray scattering profiles, each referred to as a "gene." Fifty chromosomes were initialized by randomly sampling from the respective candidate pool. In each optimization step, another 50 chromosomes were generated by exchanging one-fifth of their genes with another surviving chromosome, and another 50 chromosomes were generated by randomly mutating up to one-fifth of the genes of each surviving chromosome. A χ^2 fitness metric was enforced to evaluate fit to the experimental data[55] and rank the best 50 surviving chromosomes to be passed to the next optimization round. After 10,000 steps of optimization, the best fit chromosome, comprised of corresponding conformations whose relative weights were embedded in the theoretical average scattering, was selected for structural analysis. Details on how the representative structural models were refined are reported in the Supporting Information.

RESULTS AND DISCUSSION

Tracking pH Dependence with Equilibrium SAXS. Utilizing equilibrium SAXS, we found significant structural changes in the i-motif over the pH series. The SAXS patterns

https://doi.org/10.1021/jacs.4c11768
J. Am. Chem. Soc. 2024, 146, 33743−33752

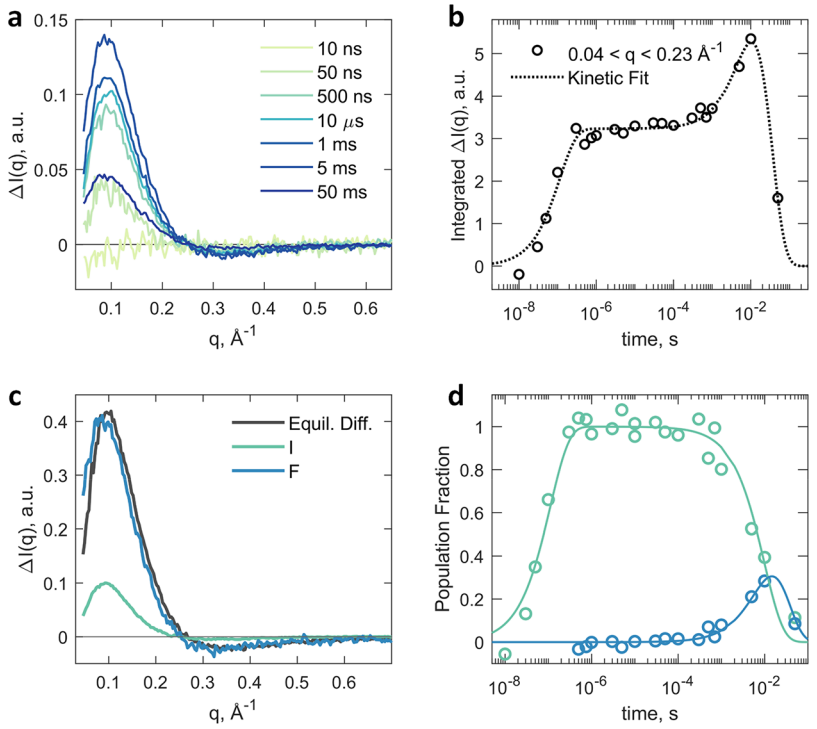

Figure 3. pH-Jump TRXSS and global analysis results. (a) Select TRXSS difference profiles spanning 10 ns to 50 ms. (b) Integrated time-resolved difference signals from 0.04 Å^{-1} < q < 0.23 Å^{-1} overlaid with kinetic fit from global analysis. (c) Species associated difference profiles for intermediate (I), transient folded (F), and between the equilibrium folded and unfolded species—determined from the equilibrium SAXS analysis (refer to Figure S4b). (d) Relative population fractions of the time-resolved species associated difference profiles: I (green) and F (blue).

for each pH are plotted in semilogarithmic scale (Figure 2a) and as dimensionless Kratky plots (Figure 2c). The dimensionless Kratky representations of the SAXS profiles normalize for the respective molecular size and radius of gyration (R_g), resulting in curves that inform unimolecular shape alone. Under acidic conditions, a noticeable single peak is observed near qR_g = 2 in the Kratky plot profiles, indicating that the i-motif oligonucleotide has a unimodal globular collapsed structure. As the pH increases toward neutral and to the upper end point of pH = 8.0, the shape of the peak broadens and transitions sharply into a profile intensity that monotonically increases with qR_g, suggesting the loss of uniform globular shape and the onset of an ensemble of disordered conformations. The reverse can be said for the overall collapse of the oligonucleotide with decreasing pH, where there is a progressive increase in the SAXS intensity (Figure 2a). To characterize the transition, singular value decomposition was applied to separate the apparent species from the background signal. Two significant components were extracted from the SAXS pH series with a sharp melting transition between the two. Subsequent population fitting using a two-state sigmoidal model resulted in a pH midpoint of 6.2 with a fwhm of 0.08 unit (Figure 2b). This sharp two-state transition agrees well with the results previously reported by Choi et al. using pH-dependent circular dichroism spectroscopy measurements (Figure S1).[14]

The R_g trends of the i-motif over the pH series provide further evidence of the coil-to-quadruplex transition as the pH is lowered. The R_g of the structural ensembles probed by SAXS can be obtained by applying Guinier analysis to the pH-dependent SAXS profiles. The resulting R_g plots (Figure 2d) show the typical values of ∼13 Å for i-motifs at acidic pHs and evidence for a disordered random coil state (∼21 Å) at neutral and basic pHs. These R_g results agree well with the experimental conclusions of Jin et al., where they reported an ensemble equilibrium R_g ranging from 14.6 Å at pH 3.99 to 22.8 Å at pH 11.2.[56] Their analysis suggested that it was necessary to consider a mixture of i-motif conformations to accurately model the structural information captured by X-ray scattering methods.[56] Thus, one cannot interpret the conformational complexity or observe intermediate states of the i-motif folding mechanism through equilibrium SAXS measurements alone.

Revealing the Early Folding Process by pH-Jump TRXSS. To elucidate the pH-responsive folding mechanism of i-motif, TRXSS offers a methodology for studying the conformational transition in real time.[31,42,44,47] A TRXSS experiment was carried out to collect pH-jump difference X-ray scattering signals, which contain information about the biomolecular structural response after deprotonation of the photoacid. Time delays between 10 ns and 50 ms were measured (Figures S5−S7). After the transient solvent response is removed, the resulting curves represent the scattering difference after the pH-jump of the oligonucleotide molecule only (Figure 3a). Upon initial investigation, a dominant increase in the TRXSS difference profile is observed between 0.04 and 0.23 Å^{-1}. The changes in this region of interest are consistent with the changes observed in the equilibrium SAXS pH series, indicative of an increase in globular secondary structure as time goes on due to the local acidification of the solution. The temporal evolution of this TRXSS difference signal was analyzed first by integrating the time series in this region of interest (see Figure 3b, for plots of the resulting signal areas). The increase in the TRXSS difference signal occurred in two steps before decreasing at the longest time delay. The accumulation of difference signal,

https://doi.org/10.1021/jacs.4c11768
J. Am. Chem. Soc. 2024, 146, 33743−33752

up to ∼1 μs, is the first sign of a transient intermediate state, which later evolved into a further signal increase on the milliseconds time scale (Figure 3b). The loss of difference signal is expected beyond 10 ms since that is the time scale on which the diffusion of protons, released in a nonequilibrium condition from the UV laser pulse and photoacid, contribute to returning the pH to the initial value (before the pH-jump). Thus, the longer time delays measured in the form of a decreasing difference signal captured i-motif unfolding due to the re-equilibration of the environment. Knowing the characteristics of the TRXSS difference scattering patterns' time evolution, the following sequential kinetic model was proposed to fit the time series:

$$U \xrightarrow{\tau_1} I \xrightarrow{\tau_2} F \xrightarrow{\tau_3} U$$

where the unfolded starting species (U) transitions to an intermediate (I) and folded species (F) sequentially, followed by the decay back to the unfolded species. The growth of the intermediate species was captured in the early time series, indicated as I, with a time constant, τ_1, of 113 ± 5 ns (Figure S8). In the late-time series, the decay of the intermediate was modeled in conjunction with the growth and decay of the pH-jump-induced folded species (F). It was found that I transitioned to F with a time constant, τ_2, of 10 ± 1 ms (Figure S9). As mentioned previously, the pH becomes more basic at long time delays due to the diffusion of protons out of the photoexcitation beam spot. This phenomenon results in a measurable decay of the pH-induced F species with a time constant, τ_3, of >23 ms (Figure S9). Since this experiment did not robustly characterize the decay of TRXSS signal beyond 10 ms, we do not capture intermediates upon unfolding from F to U nor aim to describe the experiment-specific diffusion, τ_3, more accurately. Our three-state kinetic model, with a populated intermediate species during i-motif folding, is consistent with the multiple species present in FRET fluorescence decay lifetimes.[14] By probing the early folding process, we characterized the initial folding process of the pH-driven oligonucleotide in real time. The proposed three-state mechanism for i-motif folding agrees with that presented in previous investigations of i-motif kinetics, which suggest conformational flexibility and an intermediate species.[14,27,57]

The resulting species-associated difference (SAD) patterns, extracted from global target analysis (Figure 3c) and their corresponding transient population fractions (Figure 3d) were determined (see Figures S9 and S10). Although the I SAD profile showed a small positive difference signal below 0.2 Å^{-1}, the SAD corresponding to the F species was characterized by a larger positive difference signal, implying a larger presence of higher-order folded structures similar to the SAD of the folded to unfolded at equilibrium (Figure S4b). A Bayesian indirect Fourier transform was performed on the reconstructed species-associated scattering profiles, resulting in pairwise distribution functions (PDF) (Figure 4). These PDFs contain information associated with the measured pairwise distances of atoms in the biomolecular ensemble at each state in the folding mechanism. The unfolded state is characterized by a broad distribution of distances up to the measured fully extensible distance (D_{max}) of 65 Å. The PDF of the transient intermediate species showed a slightly smaller D_{max} of 62 Å, a shape in the distribution that populates shorter characteristic distances, approximately 15 Å, and less population at longer distances. The species-associated ensemble R_g of the unfolded and pH-induced intermediate are similar, 20.5 ± 0.5 and 19.1 ± 0.3 Å,

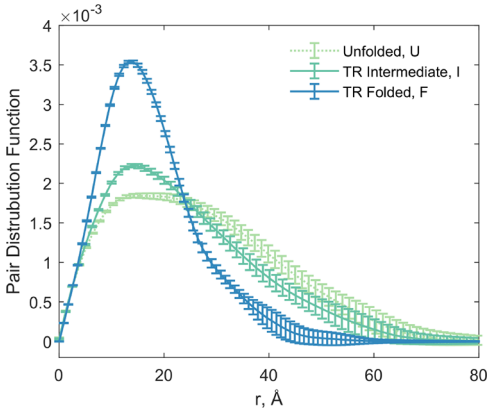

Figure 4. Pair distance distribution functions of the kinetic species.

respectively, further indicating a transition toward collapsed oligonucleotide structures with persisting extended random coil conformations. As the oligonucleotides progressed to the transient folded species (F), a significant decrease in these physical parameters was measured: a species associated with R_g of 15.2 ± 0.1 Å and D_{max} of 44 Å. The PDF of the folded state shows a large relative increase in probability density at short distances; this data is evidence for the conversion from extended oligonucleotide conformations to either partially or fully folded structures. These species-associated PDFs agree with those previously reported in a pH-dependent SAXS study of i-motif DNA.[56] Jin et al. discussed the need to consider a structural ensemble to model the scattering profiles measured; hence, this agreement between the species-associated signatures and the established equilibrium findings suggests that these transient species have ensemble conformational tendencies corresponding to the time evolution of pH-induced i-motif folding.[56]

Structural Analysis. To extract the microscopic structural information from the measured macroscopic signatures, which embed the ensemble of biomolecular electron densities, we employed an ensemble optimization method that algorithmically solved for the best combinatorial cluster to model each experimental kinetic species, *e.g.*, U, F, and I.[35,44,53,54] The results of this ensemble fitting for each kinetic species is a group of individual molecular conformers, whose averaged calculated scattering profiles best fit the experimentally determined species-associated scattering profile (see Figures S15−S17 for each scattering fit). These groups of oligonucleotide conformations were consistently achieved even while varying the initial seed of the algorithm; thus, the resulting conformations provide a means for us to understand the structural tendencies of the species-associated scattering signatures. To interpret the resulting conformational groups, two metrics, R_g and heavy-atom root-mean-square deviation (RMSD) relative to the starting i-motif structure, were chosen to cast the optimal 30 conformations for each transient species (Figure 5). As expected, the unfolded species, before the pH-jump, mostly consisted of various extended conformations of single-stranded oligonucleotides with R_g's between 18 and 20 Å (Figure 5a; see Figure S18 for examples of structures). The corresponding RMSD histogram (Figure 5d) shows that these conformations also deviated largely from a known i-motif fold by ∼2 nm. The transient intermediate species, I, was mapped to an ensemble of conformations that had comparably smaller R_g's (Figure 5b; see Figure S19 for examples of structures),

https://doi.org/10.1021/jacs.4c11768
J. Am. Chem. Soc. 2024, 146, 33743−33752

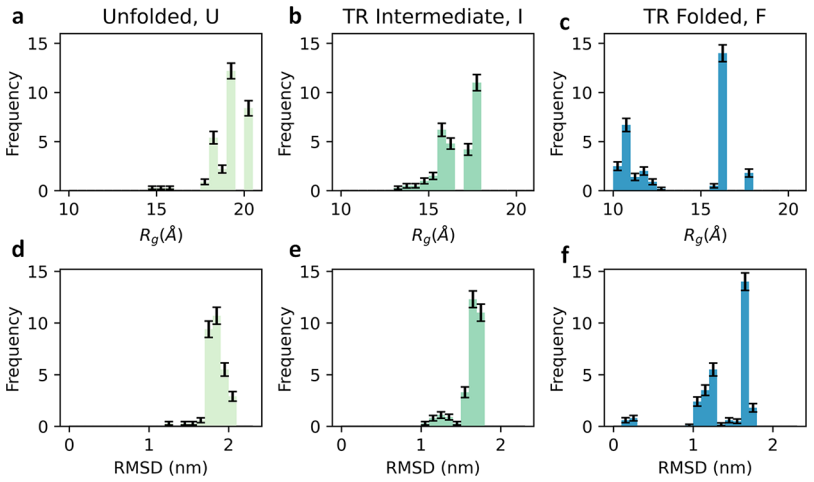

Figure 5. Histograms of species-associated ensemble structural metrics. (a–c) R_g histograms of the average conformational ensembles for each kinetic species (U, I, and F, respectively) with standard errors. (d–f) RMSD histograms of the average conformational ensembles of the corresponding species (U, I, and F, respectively) with standard errors.

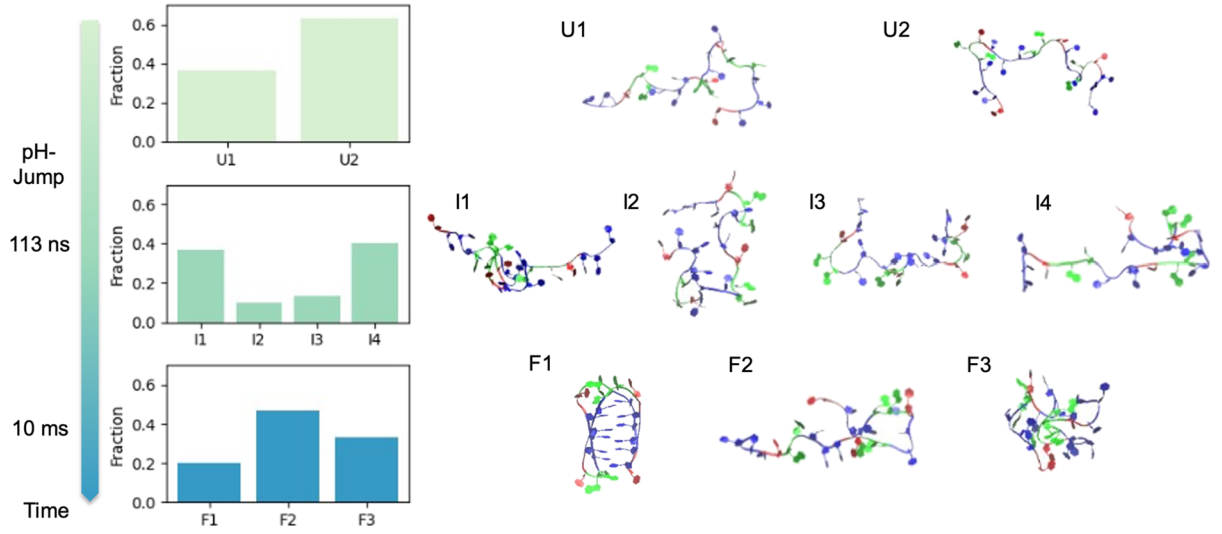

Figure 6. Population fractions of representative structures of i-motif oligonucleotide for each kinetic species: unfolded (U_i), intermediate (I_i), and folded (F_i). Oligonucleotide ribbon structures colored by nucleotide type: adenine (green), thymine (red), and cytosine (blue).

implying some partial folding and intramolecular interactions. However, the i-motif folds are not yet populated in this transient intermediate, which arose after 1 μs; rather these partially folded structures maintained RMSD's that suggest significant divergence from the desired i-motif at acidic pH's (Figure 5e). The folded species, F, captured by the pH-jump TRXSS experiment were optimally represented by a mixture of collapsed (R_g < 13 Å) and partially extended structures ($R_g \approx$ 15 Å) (Figure 5c; see Figure S20 for examples of structures). Quadruplex base-paired i-motif structures were observed for this kinetic species, reaffirmed by their small RMSD (<0.3 nm), albeit they were a small fraction of this ensemble (Figure 5f). The remaining non-i-motif structures in the folded species contribute a small R_g, close to or sometimes shorter than that of the native i-motif quadruplex conformation, suggesting the presence of structures reacting to a pH-induced collapse but not completely folded. These conformational ensembles represent structural tendencies, mapped in the context of R_g and RMSD, for the i-motif oligonucleotide as it goes from a disordered unfolded form toward a folded quadruplex, in response to the pH-jump.

To extract the molecular models for each of the kinetic species described above, we utilized hierarchical agglomerative clustering for each of the optimally determined ensembles according to the RMSDs (see Section S8 in the Supporting Information for details). It was possible to simplify the conformations obtained from the ensemble optimization method to two to four representative structures, with their corresponding population fractions readjusted (Figure 6). The unfolded species, U, is consistent with the expectations of disordered single-stranded oligonucleotide at neutral pH conditions and is represented by structures, labeled U_1 (37%) and U_2 (63%). These conformations lack intramolecular contacts and accurately reflect the nature of the oligonucleotide before the pH-jump. The intermediate species, I, exhibited a mixture of conformations, suggestive of partially folded structures (noted in Figure 5b,e). Four representative structures were the outcome of the clustering procedure, with three of the four showing signs of partial folding and intramolecular contacts. These intermediate constituents depict the possible "initial folds" of the oligonucleotide, as it adopts a smaller global shape in response to the acidic

https://doi.org/10.1021/jacs.4c11768
J. Am. Chem. Soc. 2024, 146, 33743–33752

environment. The i-motif sequence contains four cytosine-rich segments, and preliminary folds can be intrachain contacts between any two of those segments. I_1 (37%) is a partially folded conformation nucleated in the center of the strand, stemming from interactions between the two adjacent cytosine-rich segments. I_4 (40%) is a partially folded conformation with interactions formed by cytosine-rich segments at the end, bending the backbone toward a hairpin structure. The long-range interactions would result from the cytosine-rich segments at the 3′ and 5′ ends of the sequence, which is the least represented partially folded structure: I_2 (10%). The remaining disordered structures, I_3 (13%), were still picked up by the ensemble fitting, showing structural similarity to U_2 and affirming the sequential relationship between the unfolded and transient intermediate species. The long-lived intermediate species is consistent with the interpretation that partially folded or misfolded i-motif contacts are kinetically formed and must be overcome in order for the i-motif quadruplex formation to occur.[58]

In the late-time millisecond regime, our structural analysis revealed the conformations that make up the transient folded species captured by the SAD signals. Quadruplexed i-motif (F_1) was found to contribute to 20% of this ensemble, coexisting with a partially folded F_2 (47%) and drastically collapsed F_3 (33%). Why do the folded kinetic species show a minority of i-motif structures? At this time delay from the pH jump (∼20 ms), the F_1 (folded) structure is not the dominant kinetic species and must compete with conformers that are higher in energy than the equilibrium i-motif. In other words, we expect that cytosine-rich nucleotides, like the sequence investigated here, will adopt collapsed, unfolded structures when undergoing rapid switching that are fully consistent with a folded i-motif's structural characteristics, such as R_g and FRET efficiency. Furthermore, the mixture of this ensemble is consistent with the known conformational flexibility of this i-motif sequence from a previous SAXS experiment that modeled i-motifs in acidic conditions, accounting for partially folded conformations.[56] The presence of the collapsed F_3 conformation, which comprised one-third of the transient folded species, is an observation that has yet to be considered in the mechanism of early i-motif formation. The early steps of i-motif formation, in response to a rapid pH-jump, allowed for the dramatic collapse of the molecule into a globularly compact (R_g < 13 Å), yet misfolded, structure. This pH-induced collapse could give a "folded" FRET response in unbound i-motif experiments where the structure is inferred from chromophore distance, leading to multiple fluorescence decay components based on the subtle structural reorganizations in the collapsed length scale.[14,26] In addition, we anticipate the kinetic formation of these species to differ for folding experiments characterized with oligonucleotide systems tethered at one or both ends.[27] With our ensemble optimization method, we are now able to distinguish between the "collapsed yet unfolded" F_3 and the i-motif F_1 conformations as they form at overlapping time scales. We expect that the competing kinetic structures uncovered here will not only provide insight into the fundamental mechanism of i-motif folding but also the transient conformations will quantify the design space uncertainty for tunable i-motif nanomachines. Further study into i-motif sequences with different ratios of cytosine blocks to the length of the entire sequence will provide further details about the diversity of kinetic structures.

CONCLUSIONS

We directly investigated the pH-induced conformational dynamics of the i-motif using pH-jump TRXSS and complementary molecular modeling to reveal the representative structures and structural tendencies in i-motif formation. Although the conformational flexibility of the i-motif had been noted in previous studies, the early structural dynamics on submillisecond time scales had yet to be conclusively determined.[14,27,56,57,59] Furthermore, previous MD simulations remained inconclusive regarding the transient intermediates because force field parameters for noncanonical nucleic acid structures are an emerging field of research.[17,29] Here, using pH-jump TRXSS, we captured the three-state kinetics of i-motif folding in solution. The global target analysis revealed the presence of an intermediate signature that populated in 113 ns and evolved into a transiently detected folded species in 10 ms. Because of the conformational flexibility of the i-motif, multiple microscopic folding pathways were found to evolve simultaneously in response to the synchronized pH-jump trigger. Therefore, the species-associated experimental scattering signatures were ensembles that contained embedded structural information on individually distinct conformations. To extract those representative structures, ensemble fitting and clustering methods were applied to extract the representative transient conformations, which were previously unknown. We found that the transient intermediate species consisted of various partially folded conformations. Moreover, the transient folded species, prepared by the laser-induced pH-jump, was a mixture of i-motif (F1), partially folded intermediate structures (F2), and a compact, yet misfolded, trapped conformation (F3). By combining SAXS measurements, which implicitly embed global structural information and complementary atomistic modeling, we were able to explore the early folding response of the i-motif and differentiate between conformations of varying intrachain contacts. The structural elucidation of i-motifs along a pH-triggered pathway gives insight into noncanonical nucleic acid structural dynamics and quadruplex structural kinetic stabilization in biological contexts. In addition, the promise of i-motif switches using a variety of environmental triggers requires a kinetic understanding, and our study provides a template for future nanotechnology studies.

ASSOCIATED CONTENT

Supporting Information

The Supporting Information is available free of charge at https://pubs.acs.org/doi/10.1021/jacs.4c11768.

Contains details for oligonucleotide synthesis and purification, data acquisition, data processing, and analysis (PDF)

AUTHOR INFORMATION

Corresponding Authors

Kevin L. Kohlstedt − *Department of Chemistry and International Institute for Nanotechnology, Northwestern University, Evanston, Illinois 60208, United States;* orcid.org/0000-0001-8045-0930; Email: kkohlstedt@northwestern.edu

Lin X. Chen − *Department of Chemistry and International Institute for Nanotechnology, Northwestern University, Evanston, Illinois 60208, United States; Chemical Sciences and Engineering Division, Argonne National Laboratory,*

https://doi.org/10.1021/jacs.4c11768
J. Am. Chem. Soc. 2024, 146, 33743−33752

Argonne 60439 Illinois, United States; Email: l-chen@northwestern.edu

Authors

Arnold M. Chan − *Department of Chemistry and International Institute for Nanotechnology, Northwestern University, Evanston, Illinois 60208, United States*; orcid.org/0000-0002-3927-0636

Sasha B. Ebrahimi − *International Institute for Nanotechnology and Department of Chemical and Biomolecular Engineering, Northwestern University, Evanston, Illinois 60208, United States*; orcid.org/0000-0003-2752-5109

Devleena Samanta − *Department of Chemistry and International Institute for Nanotechnology, Northwestern University, Evanston, Illinois 60208, United States*; orcid.org/0000-0002-0647-7673

Denis Leshchev − *Department of Chemistry, Northwestern University, Evanston, Illinois 60208, United States*; orcid.org/0000-0002-8049-3671

Adam K. Nijhawan − *Department of Chemistry and International Institute for Nanotechnology, Northwestern University, Evanston, Illinois 60208, United States*; orcid.org/0000-0001-5527-1850

Darren J. Hsu − *Department of Chemistry, Northwestern University, Evanston, Illinois 60208, United States*; orcid.org/0000-0002-0353-7626

Madeline B. Ho − *Department of Chemistry, Northwestern University, Evanston, Illinois 60208, United States*; orcid.org/0000-0001-6351-2132

Namrata Ramani − *International Institute for Nanotechnology and Department of Material Science and Engineering, Northwestern University, Evanston, Illinois 60208, United States*

Irina Kosheleva − *Center for Advanced Radiation Sources, The University of Chicago, Chicago, Illinois 60637, United States*

Robert Henning − *Center for Advanced Radiation Sources, The University of Chicago, Chicago, Illinois 60637, United States*

Chad A. Mirkin − *Department of Chemistry, International Institute for Nanotechnology, Department of Chemical and Biomolecular Engineering, and Department of Material Science and Engineering, Northwestern University, Evanston, Illinois 60208, United States*; orcid.org/0000-0002-6634-7627

Complete contact information is available at: https://pubs.acs.org/10.1021/jacs.4c11768

Author Contributions

The manuscript was written through contributions of all authors. All authors have given approval to the final version of the manuscript.

Notes

The authors declare no competing financial interest.

■ ACKNOWLEDGMENTS

This work was supported by the National Institute of Health (NIH), under contract no. R01-GM115761. A.M.C. and M.B.H. acknowledge support from the NIH/National Institute of General Medical Sciences (NIGMS) sponsored Molecular Biophysics Training Program at Northwestern University (T32GM140995). This material is based upon work supported by the National Science Foundation under Grant DBI-2032180. S.B.E. was supported in part by the Chicago Cancer Baseball Charities and the H Foundation at the Lurie Cancer Center of Northwestern University. This research used resources of the Advanced Photon Source (APS), a U.S. DOE Office of Science User Facility operated for the DOE Office of Science by Argonne National Laboratory under contract no. DE-AC02-06CH11357. The use of BioCARS was also supported by the NIH-NIGMS under grant number R24GM111072. The content is solely the responsibility of the authors and does not necessarily represent the official views of the National Institutes of Health. Time-resolved setup at Sector 14 was funded in part through a collaboration with Philip Anfinrud (NIH/NIDDK). Optical equipment used for UV beam delivery at BioCARS was purchased with support from the Fraser lab at the University of California San Francisco. Portions of this work were performed at the DuPont-Northwestern-Dow Collaborative Access Team (DND-CAT) located at Sector 5 of the APS. DND-CAT is supported by Northwestern University, The Dow Chemical Company, and DuPont de Nemours, Inc.

■ ABBREVIATIONS

DNA, deoxyribonucleic acid; UV, ultraviolet; FRET, Forster resonant energy transfer; SAXS, small-angle X-ray solution scattering; TRXSS, time-resolved X-ray solution scattering; MD, molecular dynamics; SVD, singular value decomposition; PDF, pair distribution function; RMSD, root-mean-square deviation

■ REFERENCES

(1) Ebrahimi, S. B.; Samanta, D.; Cheng, H. F.; Nathan, L. I.; Mirkin, C. A. Forced Intercalation (FIT)-Aptamers. *J. Am. Chem. Soc.* **2019**, *141* (35), 13744−13748.

(2) Zhu, J.; Kim, Y.; Lin, H.; Wang, S.; Mirkin, C. A. pH-Responsive Nanoparticle Superlattices with Tunable DNA Bonds. *J. Am. Chem. Soc.* **2018**, *140* (15), 5061−5064.

(3) Wang, Z.-G.; Elbaz, J.; Willner, I. DNA Machines: Bipedal Walker and Stepper. *Nano Lett.* **2011**, *11* (1), 304−309.

(4) Laisné, A.; Pompon, D.; Leroy, J.-L. [C7GC4]4 Association into supra molecular i-motif structures. *Nucleic Acids Res.* **2010**, *38* (11), 3817−3826.

(5) Dong, Y.; Yang, Z.; Liu, D. DNA Nanotechnology Based on i-Motif Structures. *Acc. Chem. Res.* **2014**, *47* (6), 1853−1860.

(6) Gehring, K.; Leroy, J.-L.; Guéron, M. A tetrameric DNA structure with protonated cytosine-cytosine base pairs. *Nature* **1993**, *363* (6429), 561−565.

(7) Samanta, D.; Ebrahimi, S. B.; Kusmierz, C. D.; Cheng, H. F.; Mirkin, C. A. Protein Spherical Nucleic Acids for Live-Cell Chemical Analysis. *J. Am. Chem. Soc.* **2020**, *142* (31), 13350−13355.

(8) Modi, S.; Swetha, M. G.; Goswami, D.; Gupta, G. D.; Mayor, S.; Krishnan, Y. A DNA nanomachine that maps spatial and temporal pH changes inside living cells. *Nat. Nanotechnol.* **2009**, *4* (5), 325−330.

(9) Narayanaswamy, N.; Chakraborty, K.; Saminathan, A.; Zeichner, E.; Leung, K.; Devany, J.; Krishnan, Y. A pH-correctable, DNA-based fluorescent reporter for organellar calcium. *Nat. Methods* **2019**, *16* (1), 95−102.

(10) Anees, P.; Saminathan, A.; Rozmus, E. R.; Di, A.; Malik, A. B.; Delisle, B. P.; Krishnan, Y. Detecting organelle-specific activity of potassium channels with a DNA nanodevice. *Nat. Biotechnol.* **2024**, *42*, 1065−1074.

(11) Blackburn, E. H. Structure and function of telomeres. *Nature* **1991**, *350* (6319), 569−573.

(12) Zeraati, M.; Langley, D. B.; Schofield, P.; Moye, A. L.; Rouet, R.; Hughes, W. E.; Bryan, T. M.; Dinger, M. E.; Christ, D. I-motif

DNA structures are formed in the nuclei of human cells. *Nat. Chem.* **2018**, *10* (6), 631−637.
(13) Zhang, X.; Zhang, Y.; Zhang, W. Dynamic topology of double-stranded telomeric DNA studied by single-molecule manipulation in vitro. *Nucleic Acids Res.* **2020**, *48* (12), 6458−6470.
(14) Choi, J.; Kim, S.; Tachikawa, T.; Fujitsuka, M.; Majima, T. pH-Induced Intramolecular Folding Dynamics of i-Motif DNA. *J. Am. Chem. Soc.* **2011**, *133* (40), 16146−16153.
(15) El-Khoury, R.; Macaluso, V.; Hennecker, C.; Mittermaier, A. K.; Orozco, M.; González, C.; Garavís, M.; Damha, M. J. i-Motif folding intermediates with zero-nucleotide loops are trapped by 2′-fluoroarabinocytidine via F···H and O···H hydrogen bonds. *Commun. Chem.* **2023**, *6* (1), 31.
(16) Serrano-Chacón, I.; Mir, B.; Cupellini, L.; Colizzi, F.; Orozco, M.; Escaja, N.; González, C. pH-Dependent Capping Interactions Induce Large-Scale Structural Transitions in i-Motifs. *J. Am. Chem. Soc.* **2023**, *145* (6), 3696−3705.
(17) Panczyk, T.; Nieszporek, K.; Wolski, P. Stability and Existence of Noncanonical I-motif DNA Structures in Computer Simulations Based on Atomistic and Coarse-Grained Force Fields. *Molecules* **2022**, *27* (15), 4915.
(18) Rajendran, A.; Nakano, S.-i.; Sugimoto, N. Molecular crowding of the cosolutes induces an intramolecular i-motif structure of triplet repeat DNA oligomers at neutral pH. *Chem. Commun.* **2010**, *46* (8), 1299−1301.
(19) Cui, J.; Waltman, P.; Le, V. H.; Lewis, E. A. The Effect of Molecular Crowding on the Stability of Human c-MYC Promoter Sequence I-Motif at Neutral pH. *Molecules* **2013**, *18* (10), 12751−12767.
(20) Li, H.; Hai, J.; Zhou, J.; Yuan, G. The formation and characteristics of the i-motif structure within the promoter of the c-myb proto-oncogene. *Journal of Photochemistry and Photobiology B: Biology* **2016**, *162*, 625−632.
(21) Kim, S. E.; Hong, S.-C. Two Opposing Effects of Monovalent Cations on the Stability of i-Motif Structure. *J. Phys. Chem. B* **2023**, *127* (9), 1932−1939.
(22) McKim, M.; Buxton, A.; Johnson, C.; Metz, A.; Sheardy, R. D. Loop Sequence Context Influences the Formation and Stability of the i-Motif for DNA Oligomers of Sequence (CCCXXX)4, where X = A and/or T, under Slightly Acidic Conditions. *J. Phys. Chem. B* **2016**, *120* (31), 7652−7661.
(23) Nguyen, T.; Fraire, C.; Sheardy, R. D. Linking pH, Temperature, and K+ Concentration for DNA i-Motif Formation. *J. Phys. Chem. B* **2017**, *121* (33), 7872−7877.
(24) Nesterova, I. V.; Nesterov, E. E. Rational Design of Highly Responsive pH Sensors Based on DNA i-Motif. *J. Am. Chem. Soc.* **2014**, *136* (25), 8843−8846.
(25) Liu, D.; Balasubramanian, S. A Proton-Fuelled DNA Nanomachine. *Angew. Chem., Int. Ed.* **2003**, *42* (46), 5734−5736.
(26) Paul, S.; Hossain, S. S.; Samanta, A. Insights into the Folding Pathway of a c-MYC-Promoter-Based i-Motif DNA in Crowded Environments at the Single-Molecule Level. *J. Phys. Chem. B* **2020**, *124* (5), 763−770.
(27) Mustafa, G.; Gyawali, P.; Taylor, J. A.; Maleki, P.; Nunez, M. V.; Guntrum, M. C.; Shiekh, S.; Balci, H. A single molecule investigation of i-motif stability, folding intermediates, and potential as in-situ pH sensor. *Frontiers in Molecular Biosciences* **2022**, *9*, No. 977113.
(28) Mondal, M.; Gao, Y. Q. Microscopic Insight into pH-Dependent Conformational Dynamics and Noncanonical Base Pairing in Telomeric i-Motif DNA. *J. Phys. Chem. Lett.* **2022**, *13* (23), 5109−5115.
(29) Panczyk, T.; Wolski, P. Molecular dynamics analysis of stabilities of the telomeric Watson-Crick duplex and the associated i-motif as a function of pH and temperature. *Biophys. Chem.* **2018**, *237*, 22−30.
(30) Lee, Y.; Oang, K. Y.; Kim, D.; Ihee, H. A comparative review of time-resolved x-ray and electron scattering to probe structural dynamics. *Struct. Dyn.* **2024**, *11* (3), No. 031301.
(31) Rimmerman, D.; Leshchev, D.; Hsu, D. J.; Hong, J.; Abraham, B.; Henning, R.; Kosheleva, I.; Chen, L. X. Revealing Fast Structural Dynamics in pH-Responsive Peptides with Time-Resolved X-ray Scattering. *J. Phys. Chem. B* **2019**, *123* (9), 2016−2021.
(32) Cho, H. S.; Schotte, F.; Dashdorj, N.; Kyndt, J.; Henning, R.; Anfinrud, P. A. Picosecond Photobiology: Watching a Signaling Protein Function in Real Time via Time-Resolved Small- and Wide-Angle X-ray Scattering. *J. Am. Chem. Soc.* **2016**, *138* (28), 8815−8823.
(33) Lee, S. J.; Kim, T. W.; Kim, J. G.; Yang, C.; Yun, S. R.; Kim, C.; Ren, Z.; Kumarapperuma, I.; Kuk, J.; Moffat, K.; et al. Light-induced protein structural dynamics in bacteriophytochrome revealed by time-resolved x-ray solution scattering. *Sci. Adv.* **2022**, *8* (21), No. eabm6278.
(34) Bennett, A. L.; Edwards, R.; Kosheleva, I.; Saunders, C.; Bililign, Y.; Williams, A.; Bubphamala, P.; Manosouri, K.; Anasti, K.; Saunders, K. O.; et al. Microsecond dynamics control the HIV-1 Envelope conformation. *Sci. Adv.* **2024**, *10* (5), No. eadj0396.
(35) Kim, T. W.; Lee, S. J.; Jo, J.; Kim, J. G.; Ki, H.; Kim, C. W.; Cho, K. H.; Choi, J.; Lee, J. H.; Wulff, M.; et al. Protein folding from heterogeneous unfolded state revealed by time-resolved X-ray solution scattering. *Proc. Natl. Acad. Sci. U. S. A.* **2020**, *117* (26), 14996−15005.
(36) Lee, Y.; Lee, H.; Ihee, H. Structural dynamics of proteins explored via time-resolved x-ray liquidography. *Chem. Phys. Rev.* **2022**, *3* (4), No. 041304.
(37) Takala, H.; Björling, A.; Berntsson, O.; Lehtivuori, H.; Niebling, S.; Hoernke, M.; Kosheleva, I.; Henning, R.; Menzel, A.; Ihalainen, J. A.; et al. Signal amplification and transduction in phytochrome photosensors. *Nature* **2014**, *509* (7499), 245−248.
(38) Andersson, M.; Malmerberg, E.; Westenhoff, S.; Katona, G.; Cammarata, M.; Wöhri, A. B.; Johansson, L. C.; Ewald, F.; Eklund, M.; Wulff, M.; et al. Structural Dynamics of Light-Driven Proton Pumps. *Structure* **2009**, *17* (9), 1265−1275.
(39) Rambo, R. P.; Tainer, J. A. Super-Resolution in Solution X-Ray Scattering and Its Applications to Structural Systems Biology. *Annu. Rev. Biophys.* **2013**, *42* (1), 415−441.
(40) Rambo, R. P.; Tainer, J. A. Bridging the solution divide: comprehensive structural analyses of dynamic RNA, DNA, and protein assemblies by small-angle X-ray scattering. *Curr. Opin. Struct. Biol.* **2010**, *20* (1), 128−137.
(41) Russell, R.; Millett, I. S.; Tate, M. W.; Kwok, L. W.; Nakatani, B.; Gruner, S. M.; Mochrie, S. G. J.; Pande, V.; Doniach, S.; Herschlag, D.; et al. Rapid compaction during RNA folding. *Proc. Natl. Acad. Sci. U. S. A.* **2002**, *99* (7), 4266−4271.
(42) Nijhawan, A. K.; Chan, A. M.; Hsu, D. J.; Chen, L. X.; Kohlstedt, K. L. Resolving Dynamics in the Ensemble: Finding Paths through Intermediate States and Disordered Protein Structures. *J. Phys. Chem. B* **2021**, *125* (45), 12401−12412.
(43) Rimmerman, D.; Leshchev, D.; Hsu, D. J.; Hong, J.; Abraham, B.; Henning, R.; Kosheleva, I.; Chen, L. X. Probing Cytochrome c Folding Transitions upon Phototriggered Environmental Perturbations Using Time-Resolved X-ray Scattering. *J. Phys. Chem. B* **2018**, *122* (20), 5218−5224.
(44) Chan, A. M.; Nijhawan, A. K.; Hsu, D. J.; Leshchev, D.; Rimmerman, D.; Kosheleva, I.; Kohlstedt, K. L.; Chen, L. X. The Role of Transient Intermediate Structures in the Unfolding of the Trp-Cage Fast-Folding Protein: Generating Ensembles from Time-Resolved X-ray Solution Scattering with Genetic Algorithms. *J. Phys. Chem. Lett.* **2023**, *14* (5), 1133−1139.
(45) Graber, T.; Anderson, S.; Brewer, H.; Chen, Y.-S.; Cho, H. S.; Dashdorj, N.; Henning, R. W.; Kosheleva, I.; Macha, G.; Meron, M.; et al. BioCARS: a synchrotron resource for time-resolved X-ray science. *Journal of Synchrotron Radiation* **2011**, *18* (4), 658−670.
(46) Cammarata, M.; Levantino, M.; Schotte, F.; Anfinrud, P. A.; Ewald, F.; Choi, J.; Cupane, A.; Wulff, M.; Ihee, H. Tracking the structural dynamics of proteins in solution using time-resolved wide-angle X-ray scattering. *Nat. Methods* **2008**, *5* (10), 881−886.
(47) Rimmerman, D.; Leshchev, D.; Hsu, D. J.; Hong, J.; Kosheleva, I.; Chen, L. X. Direct Observation of Insulin Association Dynamics

with Time-Resolved X-ray Scattering. *J. Phys. Chem. Lett.* **2017**, *8* (18), 4413−4418.
(48) D.A. Case, I. Y. B.-S.; Brozell, S.R.; Cerutti, D.S.; Cheatham, T.E., III; Cruzeiro, V.W.D.; Darden, T.A.; Duke, R.E.; Ghoreishi, D.; Gilson, M.K.; Gohlke, H.; Goetz, A.W.; Greene, D.; Harris, R.; Homeyer, N.; Huang, Y.; Izadi, S.; Kovalenko, A.; Kurtzman, T.; Lee, T.S.; LeGrand, S.; Li, P.; Lin, C.; Liu, J.; Luchko, T.; Luo, R.; Mermelstein, D.J.; Merz, K.M.; Miao, Y.; Monard, G.; Nguyen, C.; Nguyen, H.; Omelyan, I.; Onufriev, A.; Pan, F.; Qi, R.; Roe, D.R.; Roitberg, A.; Sagui, C.; Schott-Verdugo, S.; Shen, J.; Simmerling, C.L.; Smith, J.; SalomonFerrer, R.; Swails, J.; Walker, R.C.; Wang, J.; Wei, H.; Wolf, R.M.; Wu, X.; Xiao, L.; York, D.M.; Kollman, P.A. *AMBER 2018*; University of California: San Francisco, 2018.
(49) Pérez, A.; Marchán, I.; Svozil, D.; Sponer, J.; Cheatham, T. E.; Laughton, C. A.; Orozco, M. Refinement of the AMBER Force Field for Nucleic Acids: Improving the Description of α/γ Conformers. *Biophys. J.* **2007**, *92* (11), 3817−3829.
(50) Phan, A. T.; Mergny, J. L. Human telomeric DNA: G-quadruplex, i-motif and Watson−Crick double helix. *Nucleic Acids Res.* **2002**, *30* (21), 4618−4625.
(51) Eastman, P.; Swails, J.; Chodera, J. D.; McGibbon, R. T.; Zhao, Y.; Beauchamp, K. A.; Wang, L.-P.; Simmonett, A. C.; Harrigan, M. P.; Stern, C. D.; et al. OpenMM 7: Rapid development of high performance algorithms for molecular dynamics. *PLOS Computational Biology* **2017**, *13* (7), No. e1005659.
(52) Schneidman-Duhovny, D.; Hammel, M.; Tainer, J. A.; Sali, A. Accurate SAXS Profile Computation and its Assessment by Contrast Variation Experiments. *Biophys. J.* **2013**, *105* (4), 962−974.
(53) Tria, G.; Mertens, H. D. T.; Kachala, M.; Svergun, D. I. Advanced ensemble modelling of flexible macromolecules using X-ray solution scattering. *IUCrJ.* **2015**, *2* (2), 207−217.
(54) Bernadó, P.; Mylonas, E.; Petoukhov, M. V.; Blackledge, M.; Svergun, D. I. Structural Characterization of Flexible Proteins Using Small-Angle X-ray Scattering. *J. Am. Chem. Soc.* **2007**, *129* (17), 5656−5664.
(55) Hsu, D. J.; Leshchev, D.; Kosheleva, I.; Kohlstedt, K. L.; Chen, L. X. Integrating solvation shell structure in experimentally driven molecular dynamics using x-ray solution scattering data. *J. Chem. Phys.* **2020**, *152* (20), No. 204115.
(56) Jin, K. S.; Shin, S. R.; Ahn, B.; Rho, Y.; Kim, S. J.; Ree, M. pH-Dependent Structures of an i-Motif DNA in Solution. *J. Phys. Chem. B* **2009**, *113* (7), 1852−1856.
(57) Dhakal, S.; Schonhoft, J. D.; Koirala, D.; Yu, Z.; Basu, S.; Mao, H. Coexistence of an ILPR i-Motif and a Partially Folded Structure with Comparable Mechanical Stability Revealed at the Single-Molecule Level. *J. Am. Chem. Soc.* **2010**, *132* (26), 8991−8997.
(58) Školáková, P.; Gajarský, M.; Palacký, J.; Šubert, D.; Renčiuk, D.; Trantírek, L.; Mergny, J.-L.; Vorlíčková, M. DNA i-motif formation at neutral pH is driven by kinetic partitioning. *Nucleic Acids Res.* **2023**, *51* (6), 2950−2962.
(59) Ashwood, B.; Lewis, N. H. C.; Sanstead, P. J.; Tokmakoff, A. Temperature-Jump 2D IR Spectroscopy with Intensity-Modulated CW Optical Heating. *J. Phys. Chem. B* **2020**, *124* (39), 8665−8677.

https://doi.org/10.1021/jacs.4c11768
J. Am. Chem. Soc. 2024, 146, 33743−33752